Optimization of Continuous Heterogeneous Models

Jiaqin Chen Vadim Shapiro

Spatial Automation Laboratory*
University of Wisconsin - Madison

June 29, 2007

Abstract

A heterogeneous model consists of a solid model and a number of spatially distributed material attributes. Much progress has been made in developing methods for construction, design, and editing of such models. We consider the problem of optimization of a heterogeneous model, and show that its representation by a continuous function defined over a constructively represented domain naturally leads to simple and effective optimization procedures. Using minimum compliance optimization problem as an example, we show that the design sensitivities are directly obtainable in terms of material and geometric parameters, which can be used in any standard gradient-based optimization procedures. The proposed approach allows both local control of the material properties and global control of geometric variations, and can be used with many existing techniques for material modeling. Numerical experiments are given to demonstrate these representational advantages.

1 Introduction

1.1 Motivation

The term *heterogeneous model* refers to a general computer representation of a (typically solid) geometric domain with one or more spatially varying attributes. It is common to view such a model as a tuple [18, 1]:

$$\langle \Omega, \mathbf{F} \rangle,$$

where $\Omega \subset \mathbb{E}^3$ is a solid model, and $\mathbf{F}$ is a collection of attribute material functions $F_i : \Omega \to \mathbb{R}^m$ which may include scalar- and tensor-valued properties, such as density, volume fractions, modulus of elasticity, conductivity, and so on.

Over the last twenty years, much of the research in geometric modeling focused on construction, design, and editing of such models. Early approaches recognized that the material attribute modeling problem is an instance of a boundary value problem and developed material representation schemes based on finite element meshing and other spatial discretizations [25, 20, 27]. But advances in design and manufacturing of functionally graded materials and related technologies also led to new modeling requirements. Discrete changes in material properties implied that both the

*Complete address: 1513 University Avenue, University of Wisconsin, Madison, WI 53706, USA. Email: jiaqinchen@wisc.edu, vshapiro@engr.wisc.edu

geometric domain Ω and material properties F_i are modeled, composed, and edited in a piecewise continuous fashion. Furthermore, material properties are usually defined by and associated with material *features* and their geometric parameters that must be explicitly available in any geometric representation of Ω. Typical engineering features may include partial or complete boundaries, regions, and datums (references). Thus, dependence on artificial spatial discretizations becomes both awkward and inefficient. Many interpolation and composition approaches for constructing and editing such feature-based material models have been proposed in the literature (see [17] for a recent and comprehensive survey of heterogeneous modeling methods and techniques).

If the representation of a geometric domain $\Omega(\mathbf{b})$ is parameterized by a set of parameters $\mathbf{b} = \{b_i\}$, it may be convenient that the attribute model $F(\Omega(\mathbf{b}))$ should inherit this parameterization. In interactive modeling situations, or when the material attribute is completely determined by the geometric features, any changes to a parameter b_i are then reflected not only in the geometric model Ω but also in the accompanying material model F. On the other hand, there are at least two practical situations where this supremacy of geometric model over the material model is undesirable:

- A number of shape design and optimization methods determine the shape Ω based on material properties F in some larger fictitious design domain $D \supset \Omega$. Popular examples in this category include homogenization and SIMP methods for topology optimization.
- Typically, a product performance measure $J(\Omega, \mathbf{F})$ is function of both geometry Ω *and* material attributes F_i, and it is important to be able to modify them independently and/or simultaneously until an optimal heterogeneous model is found.

In both of these situations, it is more reasonable to assume that the geometric domain $\Omega(\mathbf{b})$ and material attributes $F_i(\mathbf{c})$ are independently represented and parameterized, so that neither relies on or restricts the modeling space of the other. In this paper, we make this assumption and study the general problem of optimizing such heterogeneous models.

1.2 Approach and outline

It should be intuitively clear that material modeling approaches based on the spatial discretizations are not appropriate because they limit allowable shape changes and explicitly tie material representation to that of the shape model. It is less clear whether feature-based approaches may be adopted for our purposes. To simplify the exposition, we will assume specific but common representations for the geometry Ω, material functions F, and the optimization problem. In particular, we will assume that geometric domain Ω is represented implicitly as the positive hyper-halfspace $\Phi \geq 0$. We will represent the material distribution F using a linear combination of B-spline basis functions over a reference domain D which contains the geometry Ω. The B-spline representation for the material field allows continuous material variations and local control of material properties. As we will discuss in Section 2, the material field does not need to conform to the underlying geometry, reducing significantly the remodeling cost caused by geometric changes. The implicit representation for the geometry allows us to combine the material and geometry in a single formulation using the characteristic function, therefore supporting simultaneous optimization of material properties and geometry variations.

In Section 3, for the sake of concreteness, we completely formulate and solve one of the most common shape and material optimization problems using our assumed representation: minimization of compliance. We then show that both material and shape sensitivities are readily obtained and

computed from the assumed material model representation. Our prototype implementation and numerical experiments demonstrating effectiveness of the approach are discussed in Section 4. We demonstrate the application of the described optimization procedure to the SIMP material model which is commonly used in the area of topology optimization, and demonstrate a non-trivial extension of the method using simultaneous material and shape variations.

As we explain in the concluding Section 5, the proposed approach is not restricted to implicit representations of domain Ω. In fact, it applies with minimal modifications to *most* geometric representations that are constructive in the sense that they rely on a finite set of primitives Ω_i. We also discuss briefly how our approach may be combined with other feature-based material modeling approaches.

2 Continuous Material Field over Implicitly Defined Domain

2.1 Continuous Representation of the Material Field

As we discussed above, we separate the material representation from the geometric representation, i.e. the material representation does not need to conform to the actual geometry Ω. The material field $F(x)$, x is the spatial coordinate, is represented as a linear combination of basis functions $\{\chi_i(x), i = 1, \ldots, N\}$ from some complete space:

$$F(x) = \sum_{i=1}^{N} c_i \chi_i(x). \tag{1}$$

Choices of the basis functions $\{\chi_i(x)\}$ may include polynomials, trigonometric, B-splines, radial basis functions, etc. The appropriate choice of basis functions allows us to obtain desired properties. We choose linear B-spline basis functions due to their well-understood local control properties [12]. The B-spline basis functions are distributed over a uniform grid subdividing the reference domain D which contains the actual geometry Ω. The coefficients $\{c_i\}$ uniquely determine the associated material field in Expression (1). The basis function representation parameterizes the continuous material field in terms of the coefficients $\{c_i\}$, effectively transforming the material optimization problem to the problem of determining the optimal values for parameters $\{c_i\}$.

2.2 Implicit Representation for the Geometry

Implicit representations of shapes have a long tradition in geometric modeling and computer graphics, as described in several recent books [9, 47]. All such representations define a shape $\Omega \subseteq D$ implicitly in terms of non-negative values of some function $\Phi(x)$ of the spatial variable x as $\Omega = \{x \in D \,|\, \Phi(x) \geq 0\}$, where D is some predefined reference domain that contains all possible shapes Ω of interest. The boundary $\partial\Omega$ of the shape Ω is the zero level set of the function $\partial\Omega = \{x \in D \,|\, \Phi(x) = 0\}$. This definition is consistent with the notion of level set function in [36, 37, 2, 49, 48, 3], but also includes many other representations used in geometric modeling. Many techniques and transformations for constructing such representations are described in [9], including Ricci's function [29], theory of R-functions [30, 31, 38, 41], and convolution methods. More recent notable methods include exact and approximate distance fields [14, 8], blending of implicit primitives like blobs, spheres, quadrics, and local quadratics that have been fit to the points [22, 19, 24], radial basis functions with both global [46] and compact support [34, 16], and

multi-variate B-splines to represent scalar fields whose zero-sets represent the boundary of sculpted geometry [28, 35]. Implicit representations may be constructed from both Constructive Solid Geometry and Boundary Representations of geometric objects [38, 39, 40].

We adopt the implicit representation for geometric domain Ω parametrized by geometrical parameters $\mathbf{b} = \{b_j, j = 1, \ldots, M\}$. Familiar examples of implicitly defined parametric shapes include conic sections and quadric surfaces, super-ellipses and super-quadrics, tori, as well as local and global transformations of these simple shapes [9]. The corresponding functions Φ for these primitive shapes are well known. The geometric parameters (radii, focal distances, angles, positions, etc.) of these implicit representations serve as the design variables that evolve during the search for optimal shape. Parametric implicit representations for more complex shapes can be built from primitive shapes using a variety of blending, convolution, and set-theoretic techniques [9, 43, 42].

2.3 Material Fields over Implicitly Represented Geometry

We consider a material optimization problem where both the material properties $F(x)$ and the geometric domain Ω are subject to change. The optimization problem has two sets of variables, one is the set of B-spline coefficients $\{c_i\}$ representing the material distribution, the other one is the geometric parameters $\{b_j\}$ defining the geometric domain Ω. If we use the usual (Heaviside) characteristic function

$$H(\Phi) = \begin{cases} 1, & \text{if} \quad \Phi(x) \geq 0 \\ 0, & \text{if} \quad \Phi(x) < 0 \end{cases}, \tag{2}$$

as an indicator of whether a given point belongs to Ω or not, we have

$$\Omega = \{x \,|\, x \in D, H(\Phi) = 1\}. \tag{3}$$

Then the actual material distribution of interest can be obtained as $\{F(x)H(\Phi), x \in D\}$. Notice that by separating the material representation from the geometry representation, we can write the actual material field as the product of two independent functions: one is the material properties defined by B-spline basis function coefficients $\{c_i\}$ on a fixed reference domain D, the other is an indicator function of the implicit representation Φ for geometry Ω defined by geometric parameters $\{b_j\}$. As we shall see below, this decouples the material sensitivity and the shape sensitivity in the optimization process, and allows us to perform material optimization over varying geometric domains.

3 Optimization Problem

3.1 Formulation

For demonstration purposes, we focus on a compliance (strain energy) minimization problem in linear elasticity with volume constraint that has been studied by many others and is well understood[6]. We seek an optimal shape Ω and material properties such that the compliance of the structure is minimized. Suppose we use the material density $\rho(x)$ as the design variable, and the stiffness tensor E_{ijkl} is assumed to be a known function of the density, the optimization problem can be formulated

as:

$$\begin{aligned} \min_{\Omega,\rho(x)} \quad & J_0(u) = \iint_\Omega \frac{1}{2} E_{ijkl}(\rho(x))\epsilon_{ij}(u)\epsilon_{kl}(u)d\Omega \\ s.t. \quad & a(u,v) = l(v),\ \forall v \in U \\ & u|_{\Gamma_1} = u_0 \\ & \iint_\Omega \rho(x)d\Omega = V_0 \\ & 0 \le \rho(x) \le 1, \end{aligned} \tag{4}$$

where $J_0(u)$ is the total strain energy, u is the displacement field, $\epsilon_{ij}(u) = \frac{1}{2}\left(\frac{\partial u_i}{\partial x_j} + \frac{\partial u_j}{\partial x_i}\right)$ is the elastic strain, v is the virtual displacement and U is the space of all admissible displacements. The boundary $\Gamma = \Gamma_1 \cup \Gamma_2$ consists of two parts, with Dirichlet boundary condition $u = u_0$ specified on Γ_1 and boundary traction p specified on Γ_2, f is the body force. The physics of the problem is governed by the equilibrium equation $a(u,v) = l(v)$, where $a(u,v) = \iint_\Omega E_{ijkl}(\rho)\epsilon_{ij}(u)\epsilon_{kl}(v)d\Omega$, and $l(v) = \iint_\Omega fvd\Omega + \int_{\Gamma_2} pvd\Gamma$. In addition, $\iint_\Omega \rho(x)d\Omega = V_0$ is the volume (weight) constraint, and the bound constraint $0 \le \rho(x) \le 1$ reflects the fact that the material density has to be between 0 and 1.

We represent the material density $\rho(x)$ as a combination of linear B-spline basis functions $\rho(x) = \sum_{i=1}^{N} c_i\chi_i(x)$, so Problem (4) can be written as the following:

$$\begin{aligned} \min_{\Omega,c_i} \quad & J_0(u) = \iint_\Omega \frac{1}{2} E_{ijkl}(\rho)\epsilon_{ij}(u)\epsilon_{kl}(u)d\Omega \\ s.t. \quad & a(u,v) = l(v),\ \forall v \in U \\ & u|_{\Gamma_1} = u_0 \\ & \iint_\Omega \sum_{i=1}^{N} c_i\chi_i(x)d\Omega = V_0 \\ & 0 \le c_i \le 1, i = 1,\ldots,N \end{aligned} \tag{5}$$

The bound constraint for density $\rho(x)$ is automatically satisfied by setting bounds on the linear B-spline's coefficients.

The geometry Ω is to be determined in Problem (5). With the implicit representation Φ (with parameters $\{b_j\}$) for the domain Ω, we can utilize the characteristic function $H(\Phi)$ to transform the integrals in Problem (5) to integrals over the reference domain D. Therefore, Problem (5) can

be reformulated as:

$$\begin{aligned} \min_{b_j,c_i} \quad & J_0(u) = \iint_D \frac{1}{2} E_{ijkl}(\rho)\epsilon_{ij}(u)\epsilon_{kl}(u)H(\Phi)d\Omega \\ s.t. \quad & a(u,v,\Phi) = l(v,\Phi),\ \forall v \in U \\ & u|_{\Gamma_1} = u_0 \\ & \iint_D \left(\sum_{i=1}^{N} c_i\chi_i(x)\right) H(\Phi)d\Omega = V_0 \\ & 0 \le c_i \le 1, i = 1,\ldots,N, \end{aligned} \tag{6}$$

where $a(u,v,\Phi) = \iint_D E_{ijkl}(\rho)\epsilon_{ij}(u)\epsilon_{kl}(v)H(\Phi)d\Omega$, $l(v,\Phi) = \iint_D fvH(\Phi)d\Omega + \int_{\Gamma_2} pvd\Gamma$. Notice that in this formulation, all integrations are now on domain D. Problem (6) is a fully parametrized optimization problem in terms of geometric parameters $\{b_j\}$ and B-spline coefficients $\{c_i\}$. The explicit parametrization allows easy sensitivity analysis, as shown in Section 3.3.

3.2 Algorithm

Problem (6) is an explicitly parameterized optimization problem. In principle, many optimization methods may be used to solve the problem. Since the constraints in Problem (6) address different design concerns, we choose to treat them differently in the optimization procedure.

The equilibrium equation and boundary conditions are determined by the underlying linear elasticity problem, which is typically solved by some external structural analysis method. In the optimization process, we use a meshfree analysis technique (see Section 4.1) to solve the elasticity problem at each step so that the equilibrium equation and boundary conditions are automatically satisfied. The solution field also provides the evaluations of the objective function and its sensitivity at each step.

While an equality volume constraint is usually difficult to enforce during the optimization process, we use the augmented Lagrangian multiplier method, which is well understood and is widely used (for example, see [23]). By imposing the volume constraint as a penalty term in the objective function, we obtain the following augmented Lagrangian subproblem:

$$\begin{aligned} \min_{b_j,c_i} \quad & J(u) = \iint_D \frac{1}{2} E_{ijkl}(\rho)\epsilon_{ij}(u)\epsilon_{kl}(u)H(\Phi)d\Omega \\ & \qquad +\lambda\left(\iint_D \sum_{i=1}^{N} c_i\chi_i(x)H(\Phi)d\Omega - V_0\right) + \frac{1}{2\gamma}\left(\iint_D \sum_{i=1}^{N} c_i\chi_i(x)H(\Phi)d\Omega - V_0\right)^2 \\ s.t. \quad & a(u,v,\Phi) = l(v,\Phi),\ \forall v \in U \\ & u|_{\Gamma_1} = u_0 \\ & 0 \le c_i \le 1, i = 1,\ldots,N, \end{aligned} \tag{7}$$

where λ is the Lagrangian multiplier and γ is a pre-defined parameter (typically a very small number). At each iteration, we fix λ and solve the subproblem (7) for $\{c_i\}$ and $\{b_j\}$, then we update λ and check for termination criteria. If the termination criteria are not satisfied, we go to the next iteration.

To solve subproblem (7), we still need to consider the bound constraints $0 \le c_i \le 1$. The

number of these constraints is very large in our problem. For example, if we represent the material field on a 50×50 grids in two dimension, then we have 2500 B-spline coefficients, therefore 5000 constraints! It is very challenging for most optimization algorithms to handle such a large number of constraints. In our implementation, we choose to modify the stiffness tensor as the following:

$$E_{ijkl}(\rho(x)) = \begin{cases} E_{ijkl}(\rho = 1) & \text{if} \quad \rho(x) > 1 \\ E_{ijkl}(\rho) & \text{if} \quad 1 \geq \rho(x) \geq 0 \\ E_{ijkl}(\rho = 0) & \text{if} \quad \rho(x) < 0 \end{cases}, \tag{8}$$

and handle these constraints as a post process. If the update of some coefficient results in the violation of the corresponding bound constraint, we set it to be the corresponding upper or lower bound. This is physically intuitive, since reaching the upper bound implies adding as much material as possible (therefore we set $c_i = 1$); similarly, reaching the lower bound suggests removing the material (and therefore setting $c_i = 0$). This strategy is similar to the gradient-projection method (see [23]) from the optimization point of view. The main difference is that every time we hit the bound along the search direction, we restart searching from the hitting point instead of bending the search direction.

The augmented Lagrangian subproblem (7) is solved by the conjugate gradient method. Conjugate gradient method is one of the most useful techniques for solving large scale linear systems of equations and can also be adapted to solve nonlinear optimization problems. It is very appealing because in each iteration only the evaluations of the objective function and its gradient are required, no matrix operations are performed and only a few vectors need to be stored [23]. The method is well suited for the formulated large scale optimization problem, and the gradient information can be computed as shown in Section 3.3. The Polak-Ribière conjugate gradient method is adopted in our implementation. The details and convergence studies of Polak-Ribière conjugate gradient method can be found in many standard textbooks, for example, see [23].

The main algorithm consists of the following steps:

Step 1: Initialize the B-spline coefficients c_i and geometrical parameters b_j, choose λ and γ.

Step 2: Use conjugate gradient method to solve Problem (7)

(2.1) Solve the equilibrium equation with boundary conditions.

(2.2) Calculate gradient ∇J and use it as the initial search direction.

(2.3) Construct a series of search directions until the solution is found. The termination criteria is defined as $\left|\frac{\Delta J}{J}\right| \leq \epsilon$, where ϵ is a predefined small positive number.

(2.4) Reset the values for c_i to be the corresponding bounds if they are violated.

Step 3: Update Lagrangian multiplier

$$\lambda = \lambda + \frac{1}{\gamma}\left(\iint_D \sum_{i=1}^{N} c_i \chi_i(x) H(\Phi) d\Omega - V_0\right)$$

Step 4: Check termination condition. If not satisfied, go to *Step* 2. The termination criteria is defined as $\left|\frac{\Delta \lambda}{\lambda}\right| \leq \delta$, where δ is a predefined small positive number.

3.3 Sensitivity Analysis

We now present the sensitivity analysis for the augmented Lagrangian subproblem (7). Since our design variables are material parameters $\{c_i\}$ and geometric parameters $\{b_j\}$, we seek the gradient $\nabla J = \left[\frac{dJ}{dc_1}, \ldots, \frac{dJ}{dc_N}, \frac{dJ}{db_1}, \ldots, \frac{dJ}{db_M}\right]$. We assume that the body force f and the boundary traction p are independent of the design.

Since $\{c_i\}$ and $\{b_j\}$ are two independent sets of variables, we can separate $\{\frac{dJ}{dc_i}\}$ and $\{\frac{dJ}{db_j}\}$ during differentiation. In Problem (7), the displacement field u depends on the variables c_i and b_j as well and it is not obvious how to obtain the derivatives $\frac{du}{dc_i}$ and $\frac{du}{db_j}$. However, we can use the adjoint method [15], where these derivatives are not computed explicitly. In addition, the compliance minimization problem for linear structures is self-adjoint, and the derivative of the compliance J_0 with respect to c_i can be obtained as [6]:

$$\frac{dJ_0(u)}{dc_i} = \iint_D -\frac{1}{2}\frac{dE_{ijkl}(\rho)}{dc_i}\epsilon_{ij}(u)\epsilon_{kl}(u)H(\Phi)d\Omega. \tag{9}$$

Since $\frac{dE_{ijkl}(\rho)}{dc_i} = \frac{dE_{ijkl}(\rho)}{d\rho} \cdot \frac{d\rho}{dc_i} = \frac{dE_{ijkl}(\rho)}{d\rho} \cdot \chi_i(x)$, we have

$$\frac{dJ_0(u)}{dc_i} = \iint_D -\frac{1}{2}\frac{dE_{ijkl}(\rho)}{d\rho}\chi_i(x)\epsilon_{ij}(u)\epsilon_{kl}(u)H(\Phi)d\Omega. \tag{10}$$

Using the result from [11], the sensitivity $\{\frac{dJ_0}{db_j}\}$ can be obtained as:

$$\frac{dJ_0(u)}{db_j} = \int_{\partial\Omega_j} \left[fu + div(pun) - \frac{1}{2} E_{ijkl}(\rho)\epsilon_{ij}(u)\epsilon_{kl}(u) \right] \frac{1}{|\nabla\Phi|} \frac{d\Phi}{db_j} d\Gamma, \tag{11}$$

where Ω_j is the portion of the zero set of Φ corresponding to parameter b_j, i.e., the moving boundary of Ω with respect to parameter b_j.

Since

$$\frac{d}{dc_i}\left(\iint_D \sum_{i=1}^{N} c_i\chi_i(x) H(\Phi) d\Omega - V_0 \right) = \iint_D \chi_i(x) H(\Phi) d\Omega \tag{12}$$

and

$$\frac{d}{db_j}\left(\iint_D \sum_{i=1}^{N} c_i\chi_i(x) H(\Phi) d\Omega - V_0 \right) = \int_{\partial\Omega_j} \sum_{i=1}^{N} c_i\chi_i(x) \frac{1}{|\nabla\Phi|} \frac{d\Phi}{db_j} d\Gamma, \tag{13}$$

it is easy to see that

$$\frac{dJ(u)}{dc_i} = \iint_D \left[-\frac{1}{2}\frac{dE_{ijkl}(\rho)}{d\rho}\epsilon_{ij}(u)\epsilon_{kl}(u) + \lambda + \frac{1}{\gamma}\left(\iint_D \sum_{i=1}^{N} c_i\chi_i(x) H(\Phi) d\Omega - V_0 \right) \right] \chi_i(x) H(\Phi) d\Omega \tag{14}$$

and

$$\begin{aligned} \frac{dJ(u)}{db_j} = \int_{\partial\Omega_j} \Bigg[& fu + div(pun) - \frac{1}{2} E_{ijkl}(\rho)\epsilon_{ij}(u)\epsilon_{kl}(u) \\ & + \lambda \sum_{i=1}^{N} c_i\chi_i(x) + \frac{1}{\gamma} \sum_{i=1}^{N} c_i\chi_i(x) \left(\iint_D \sum_{i=1}^{N} c_i\chi_i(x) H(\Phi) d\Omega - V_0 \right) \Bigg] \frac{1}{|\nabla\Phi|} \frac{d\Phi}{db_j} d\Gamma. \end{aligned} \tag{15}$$

Once the displacement field u is known, the computation of Expression (14) and (15) involves only differentiation, boundary and volume integration. Therefore, the computation of the gradient ∇J is straightforward and can be implemented in any systems which support these operations.

4 Experimental Results

In this section we briefly discuss our numerical implementation of the above material optimization procedures and show numerical experiments to illustrate the effectiveness of the proposed method for the problem of topology optimization. In all examples, we adopt the SIMP (Solid Isotropic Material with Penalty) stiffness model for the material (tensor) properties $E_{ijkl}(\rho)$ as a function of material density. The SIMP method has been widely accepted in the area of topology optimization due to its conceptual simplicity and computational efficiency [4, 6, 5, 44]. The SIMP model uses the power-law

$$E_{ijkl}(\rho(x)) = E^0_{ijkl}\rho(x)^\alpha, \quad 0 \le \rho(x) \le 1, \tag{16}$$

where E^0_{ijkl} is the stiffness tensor of the base material. The derivative $\frac{dE_{ijkl}(\rho)}{d\rho}$ in Expression (14) can be easily obtained as $\frac{dE_{ijkl}(\rho)}{d\rho} = \alpha E^0_{ijkl}\rho(x)^{\alpha-1}$. The power $\alpha > 1$ has the effect of penalizing intermediate densities. The necessary conditions of α for the material to be physically realizable has been studied in [5], which we will not discuss in this paper. By making the intermediate densities less economic in the power-law model, the SIMP penalizes the intermediate densities and drives the structure to a near 0-1 design during the optimization process. Note however that the formulation of the sensitivity does not depend on SIMP and can be used with other models of material properties.

4.1 Meshfree Implementation

The algorithm described in Section 3.2 can be implemented in many meshfree environments that support stress/strain analysis, allow some programmability for parametric functions, and provide tools for differentiation, and boundary and volume integration. Here we briefly describe how the proposed approach is implemented using the RFM method (R-function method) [45, 41] and used earlier to solve the problems with shape deformations and moving boundary conditions [43].

Since we represent the boundary of a geometric domain by the zero level set of an evolving scalar function, it is natural to use an engineering analysis method that can work with the same geometric representation. The RFM method, a meshfree method with approximate distances, is well suited for the task. This method is based on the idea that a physical field can be represented by a generalized Taylor series expansion by powers of an approximate distance field to the boundary [31, 32, 33]. Once such distance fields are constructed, they can be used to construct solutions to boundary value problems that satisfy the prescribed boundary conditions exactly on all points where the distance field vanishes. The remainder term in the Taylor series contains degrees of freedom necessary to approximate differential equation(s), and it also assures completeness of the solution [33]. The method is essentially meshfree, though a background mesh may be used for integration and visualization purposes. A complete programming environment supporting construction, differentiation, and integration of all required functions at run time is described in [45].

In the context of the structural analysis problem solved in this paper, we represent components of the displacement vector $\mathbf{u} = (u_1, u_2)$ as products of two functions $u_i = \omega_i \Psi_i$, $i = 1, 2$, where ω_i are distance functions to the fixed portions of the boundary of the domain Ω, and functions $\Psi_i = \sum_{j=1}^{k} a_j^{\Psi_i} \xi_j$ are linear combinations of basis functions used to approximate the solution of the differential equation. Basis functions $\{\xi_j\}_{j=1}^k$ can be chosen from B-splines, polynomials, radial basis functions or even finite elements. Generally, these basis functions can be defined on a grid that does not conform to the geometric domain and are not related to the basis functions used to construct the material field ρ. In this paper we approximate components of the displacement vector using a uniform cartesian grid of bilinear B-splines. Numerical values of the coefficients $a_j^{\Psi_i}$ are determined by a standard technique that requires minimization of an energy functional [50]. As a result, we obtain a system of linear algebraic equations whose solution gives numerical values of the coefficients $a_j^{\Psi_i}$. Assembly of the matrix and vector of this system of equations requires differentiation of the approximate distance fields ω_i and basis functions with respect to spatial coordinates and integration over the non-meshed geometric domain and its boundary represented by a level set function. Use of B-splines as basis functions results in matrices that possess block-

diagonal sparse structure. Algebraic systems with such matrices can be efficiently solved by a conjugate gradient algorithm [26]. Once numerical values of the coefficients $a_j^{\Psi_i}$ are computed, they are substituted into the expressions for components of the displacement vector $\mathbf{u}$.

4.2 SIMP Examples

The first example is a short cantilever beam, the second example is a Messerschmitt-Boelkow-Blohm (MBB) beam. Both examples are benchmark problems which have been widely used in the literature [13]. The third example is a 3-hole bracket design problem. Compared to the cantilever beam and MBB beam which are defined on a rectangular domain, the bracket has a more complicated design domain. In contrast to the spatially discretized representations that require complex meshes for complicate geometries, the continuous material representation over the implicitly represented geometry does not demand any additional effort as the complexity of the geometry increases. The fourth example is also a cantilever beam, but it is defined on a varying geometric domain with a moving circular hole. Both the material distribution and the position of the hole need to be determined. The fifth example is a stepped cantilever beam where the material density and the heights of the steps need to be determined. In all examples, uniform rectangular grids are imposed on the background for supporting the basis functions representing the material field (Section 2.1) and the basis functions representing the displacement field (Section 4.1). This grid is also used for numerical integration. All examples are plane stress problems with material properties as follows: Young's elasticity modulus for base material $E^0 = 1$, and Poisson's ratio $\nu = 1/3$. The power α in the SIMP model is chosen to be 3. The body force is assumed to be zero.

Example 1: Cantilever beam

Figure 1 shows a classic short cantilever beam design problem defined on a rectangular design domain D of length $L = 0.1$, height $H = 0.05$. The thickness of the plate is $t = 0.0025$. A distributed force $p = 200$ is applied in an interval of 0.005 around the middle point of the right edge of D and the left edge of D is fixed. The volume constraint (area of the structure) is set to be one half of the design domain. We use uniformly distributed material $\rho = 1$ (i.e. $c_i = 1, i = 1, \ldots, N$) over the design domain as the initial design.

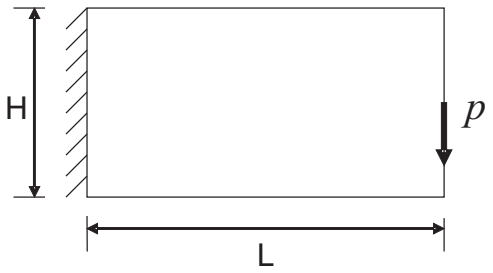

Figure 1: Problem definition of a cantilever beam.

Figure 2 shows the optimal material distribution of the cantilever beam from different grid sizes. The final designs are near 0-1 designs due to the penalization of the SIMP material model. In contrast to results from finite element based methods [6, 13], the structures obtained are free of checkerboard patterns due to the continuous material representation. We notice that material

distributions on finer grids (therefore, with more degrees of freedom) tend to generate finer structures with more complex topology and smoother boundaries. This phenomenon is often referred to as mesh-dependence in the literature [6, 13]. But visually, this mesh dependence appears to be less prominent than that observed in similar computations with from classical finite element based methods. Table 1 lists values of the objective function and the area of the optimal structures in Figure 2. We see that with finer grids, the structure has a slightly better performance (lower value of the objective function), as expected.

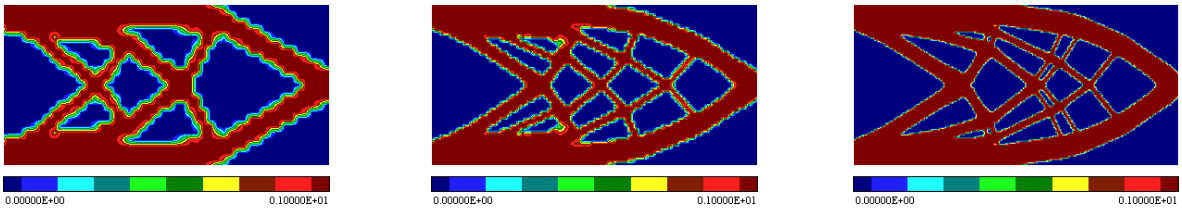

(a) 50×25 grid (b) 100×50 grid (c) 200×100 grid

Figure 2: The optimal structures of the cantilever beam from different grid sizes.

grid size	area	total strain energy
50×25	2.50013e-3	1.35270e+4
100×50	2.50115e-3	1.28726e+4
200×100	2.49983e-3	1.22711e+4

Table 1: The objective (total strain energy) and the area of the optimal cantilever beam.

Example 2: MBB beam

Figure 3 shows a MBB beam design problem on D of length $L = 6$, height $H = 1$. The thickness of the plate is $t = 0.1$. A distributed force $p = 100$ is applied in an interval of 0.12 around the middle point of the top edge of D. The volume constraint is half the area of the design domain. Uniformly distributed material $\rho = 1$ over the design domain is used as the initial design.

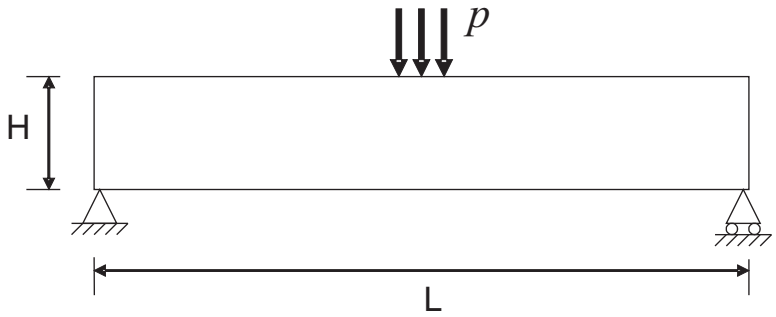

Figure 3: Problem definition of a MBB beam.

Figure 4 shows the optimal structures of the MBB beam from different grid sizes. As in the

first example, the optimal structures are free of checkerboard patterns and almost 0-1 designs. The mesh dependence is even less noticeable. Table 2 lists values of the objective function and the area of the optimal structures in Figure 4. Again we see that the structure generated from fine grids has slightly better performance.

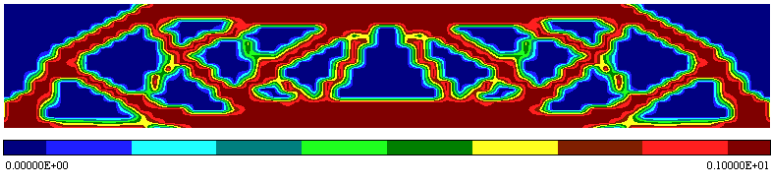

(a) 60×20 grid, with line search

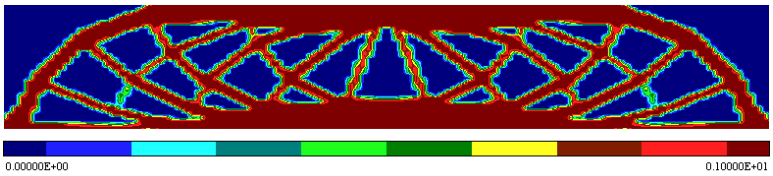

(b) 120×40 grid, with line search

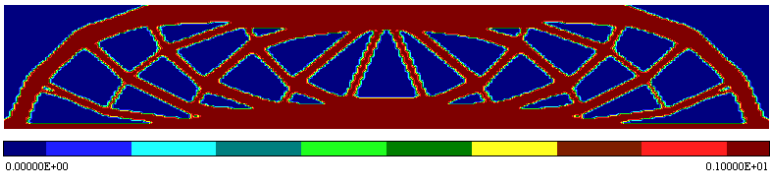

(c) 240×80 grid, with line search

Figure 4: The optimal stuctures of the MBB beam from different grid sizes.

grid size	area	total strain energy
60×20	3.00386	6.35452e+4
120×40	3.00278	6.27174e+4
240×80	2.99862	6.05220e+4

Table 2: The objective and the area of the MBB beam.

Example 3: 3-hole bracket

Figure 5 shows the design domain of a 3-hole bracket. The rectangle is of length $L = 0.1$, height $H = 0.1$. The radius of the three holes is $r = 0.01$ and the holes are fixed with $d = 0.02$. The thickness of the plate is $t = 0.0025$. A distributed force $p = 200$ is applied along the bottom half circle of the right hole, the left two holes are fixed, as shown in Figure 5. The volume constraint is $V = 0.003$. We use uniformly distributed material $\rho = 1$ as the initial design.

Figure 6 shows the optimal structures of the 3-hole bracket from different grid sizes. Though the design domain is more complicated, it is treated in our method in the same way as previous

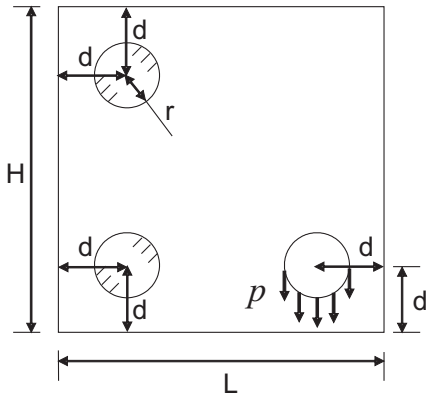

Figure 5: Problem definition of a 3-hole bracket.

examples: B-spline basis functions are posed on background rectangular grids to approximate the material field and the meshfree analysis satisfies the boundary conditions automatically. To "protect" the three holes, a tolerance zone is put around the three holes and the coefficients of B-splines basis functions that have support intersecting with this tolerance zone are fixed during the optimization process. Table 3 lists values of the objective function and the area of the optimal structures in Figure 6.

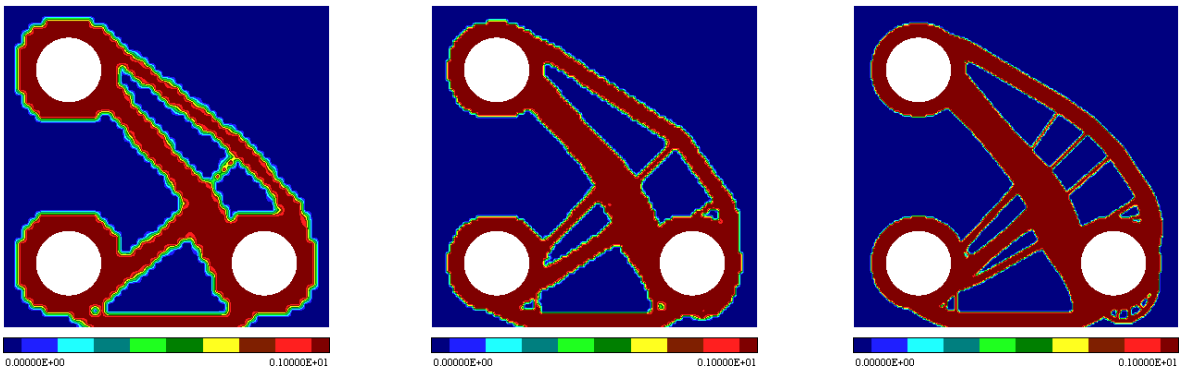

(a) 50×50 grid (b) 100×100 grid (c) 200×200 grid

Figure 6: The optimal structures of the 3-hole bracket from different grid sizes.

Example 4: Cantilever beam with a moving hole

Figure 7 shows the design domain of a short cantilever beam. The design domain has a circular hole whose position coordinates are geometric parameters that are subject to optimization. The length of the rectangle is $L = 0.1$, the height is $H = 0.05$. The thickness of the plate is $t = 0.0025$. The radius of the hole is $r = 0.0075$ and the initial position of the hole is $x_c = 0.03, y_c = 0.0125$. A distributed force $p = 200$ is applied in an interval of 0.005 around the middle point of the right edge of D and the left edge of D is fixed. The volume constraint is $V = 0.025$. Uniformly distributed material $\rho = 1$ is used as the initial design.

In this example, the position of the hole and the material distribution are optimized simuta-

grid size	area	strain energy
50×50	3.00229e-3	9.16768e+4
100×100	3.00925e-3	7.68538e+4
200×200	2.99114e-3	7.20218e+4

Table 3: The objective and the area of the 3-hole bracket.

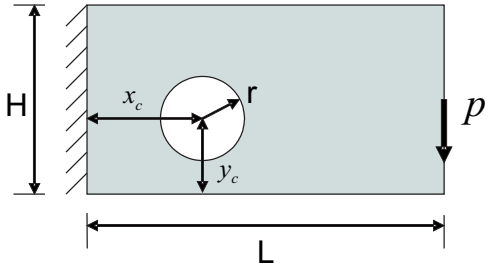

Figure 7: Problem definition of a cantilever beam with a hole.

neously. Figure 8 shows the optimal structures from different grid sizes and Table 4 lists values of the objective function, the area of the optimal structures, and the final coordinates of the hole.

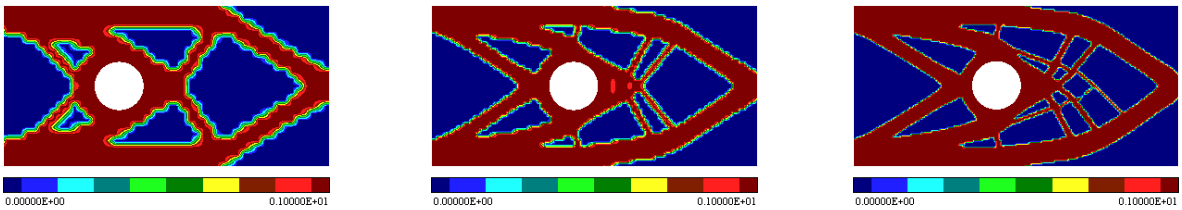

(a) 50 × 25 grid (b) 100 × 50 grid (c) 200 × 100 grid

Figure 8: The optimal structures of the one hole cantilever beam from different grid sizes.

Example 5: Stepped cantilever beam

Figure 9(a) shows the design domain of a short cantilever beam. The design domain consists of three segments (steps) whose heights are subject to optimization. The length of the rectangle is $L = 0.1$, the height is $H = 0.05$. $L_1 = 0.03$, $L_2 = 0.04$, $L_3 = 0.03$. The thickness of the plate is $t = 0.0025$. A distributed force $p = 200$ is applied in an interval of 0.005 around the middle point of the right edge of D and the left edge of D is fixed. The volume constraint is $V = 0.025$. The initial heights of the three segments are $h_1 = h_2 = h_3 = 0.025$, and the initial material density is $\rho(x) = 0.5$. Figure 9(b) and 9(c) show the initial design and the optimal structure respectively.

grid size	area	strain energy	x_c	y_c
50×25	2.50110e-3	1.36148e+4	3.54749e-2	2.49849e-2
100×50	2.50183e-3	1.27441e+4	4.36144e-2	2.49981e-2
200×100	2.49845e-3	1.23955e+4	4.41646e-2	2.51398e-2

Table 4: The objective, area and the final coordinates of the hole in the one-hole cantilever beam.

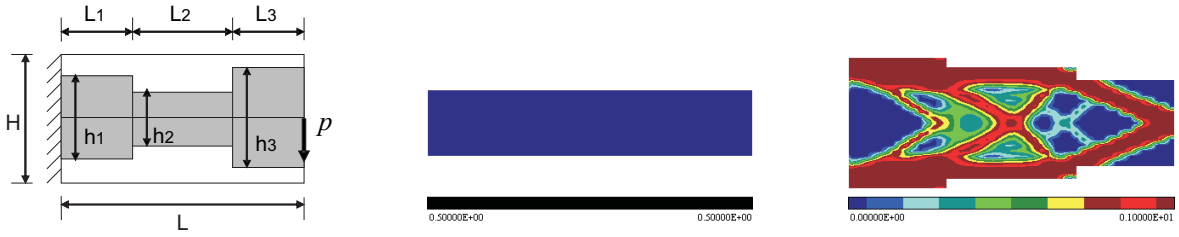

(a) the problem definition (b) the initial design (c) the optimal design

Figure 9: The optimization of a stepped cantilever beam: (a) the design domain, (b) the initial design with uniform density $\rho = 0.5$, (c) the optimal design.

5 Conclusions

5.1 Summary

We proposed a method for representation and optimization of heterogenous models. The key feature of the method is the separation of the material representation and the geometry representation. Representing the continuous material field using B-spline basis functions gives a smooth material field and allows local controls of the material properties. The implicit representation for geometry handles geometrical deformations by changing a few geometric parameters. Due to the separate representations, the material field does not need to conform to the geometry domain, and therefore no particular spatial discretization is required.

We have shown that material sensitivity and shape sensitivity are easily decoupled, supporting simultaneous material and shape optimization. The method was fully implemented in a particular meshfree framework, but it is general enough to be implemented in other computational environments with minimum requirements. Our numerical experiments for the minimum compliance problem and SIMP material model produce results that are at least as good as any published in the literature to date. In particular, we notice the absence of any numerical artifacts, such as checkerboard patterns reported by many others [6, 13]. This superior numerical behavior may be attributed to built-in continuity of the material field [21]. Furthermore, to the authors' knowledge, until now SIMP has not been formulated or implemented with simultaneously changing globally parameterized geometric domain.

5.2 Extensions

It should be clear that proposed method can be applied to any material model and extended to other structural design problems. Any gradient-based methods can be used to solve the optimization problem. It is less obvious that the proposed methods can be used with most geometric

representations and feature-based heterogeneous models.

The implicit representation of the geometry was used in this paper for two convenience purposes: to define the characteristic function $H(\Phi)$, and to derive the term $\frac{1}{|\nabla\Phi|}\frac{d\Phi}{db}$ in Equation (11). It is clear that the characteristic function computation is supported by any unambiguous representation of a solid through standard point membership classification (PMC) algorithms. Furthermore, we have recently shown [10] that the derivation of sensitivity in section 3.3 only relies on the *existence* of implicit representations, but in fact it does not matter whether the primitive is represented implicitly, parametrically, variationally, or procedurally. Also, we show in [10] that the term $\frac{1}{|\nabla\Phi|}\frac{d\Phi}{db}$ is equivalent to the normal component of the boundary velocity v_n. The proposed approach applies as long as we are able to compute the shape (design) velocity v_n in the direction normal to the primitive's boundary. Once the primitive velocities are computed based on the properties and representations of the individual primitives, they can all be used simultaneously within the framework described in this paper. In this sense, the proposed approach to optimization of heterogeneous models can be used with most geometric representations.

As we already mentioned in the introduction, the separation of material representation from geometry comes at a price: the changes in geometric parameters do not propagate into the material representation, undermining the benefits of the feature-based approach to material modeling. It is proposed in [7] that the material field may be represented as a sum of two independent fields: $F = P + R$, where the $P(\mathbf{b})$ interpolates the material properties prescribed at the features of Ω, while $R(\mathbf{c})$ is a linear combination of B-splines that may be used to control local material properties. Such representation of material field may support both interactive design of heterogeneous models where the material properties follow the geometric parameters and material optimization at the points of the domain that are sufficiently far away from the material features.

Acknowledgements

This works was supported in part by the National Science Foundation grants CMMI-0323514, CMMI-0500380, CMMI-0621116, OCI-0636206, and Wisconsin Industrial & Economic Development Research Program (I&EDR).

References

[1] V. Adzhiev, E. Kartasheva, T. Kunii, A. Pasko, and B. Schmitt. Hybrid Cellular-functional Modeling of Heterogeneous Objects. *Journal of Computing and Information Science in Engineering*, 2:312, 2003.

[2] G. Allaire, F. Jouve, and A. M. Toader. Structural optimization using sensitivity analysis and a level-set method. *Journal of Computational Physics*, 194:363–393, 2004.

[3] T. Belytschko, S. P. Xiao, and C. Parimi. Topology optimization with implicit functions and regularization. *International Journal for Numerical Methods in Engineering*, 57:1177–1196, 2003.

[4] M. P. Bendsøe. Optimal shape design as a material distribution problem. *Structural Optimization*, 1:193–202, 1989.

[5] M. P. Bendsøe and O. Sigmund. Material interpolations in topology optimization. *Archive of Applied Mechanics*, 69:635–654, 1999.

[6] M. P. Bendsøe and O. Sigmund. *Topology Optimization: Theory, Methods and Applications*. Springer Verlag, Berlin Heidelberg, 2003.

[7] A Biswas, S. Fenves, V. Shapiro, and R. Sriram. Representation of Heterogeneous Material Properties in Core Product Model. *Engineering with Computers*, 2007. in press.

[8] A. Biswas and V. Shapiro. Approximate distance fields with non-vanishing gradients. *Graphical Models*, 66(3):133–159, May 2004.

[9] J. Bloomenthal. *Introduction to Implicit Surfaces*. Morgan Kaufmann Publishers, 1997.

[10] J. Chen, M. Freytag, and V. Shapiro. Shape sensitivity of constructive representations. In *Proceedings of the 2007 ACM Symposium on Solid and Physical Modeling*, pages 85 – 95. ACM Press, 2007.

[11] J. Chen, V. Shapiro, K. Suresh, and I. Tsukanov. Shape optimization with topological changes and parametric control. *International Journal of Numerical Methods in Engineering*, 71(3):313–346, 2007.

[12] Carl de Boor. *A Practical Guide to Splines*. Springer-Verlag, 2001.

[13] H. A. Eschenauer and N. Olhoff. Topology optimization of continuum structures: A review. *Applied Mechanics Review*, 54:331–390, 2001.

[14] Sarah F. Frisken, Ronald N. Perry, Alyn P. Rockwood, and Thouis R. Jones. Adaptively sampled distance fields: A general representation of shape for computer graphics. In *Proceedings of the ACM SIGGRAPH Conference on Computer Graphics*, pages 249–254, 2000.

[15] E. J. Haug, K. K. Choi, and V. Komkov. *Design Sensitivity Analysis of Structural Systems*. Academic Press, New York, NY, 1986.

[16] N. Kojekine, I. Hagiwara, and V. Savchenko. Software tools using csrbf's for processing scattered data. *Computers and Graphics*, 27(2), 2003.

[17] XY Kou and ST Tan. Heterogeneous object modeling: A review. *Computer-Aided Design*, 39(4):284–301, 2007.

[18] V. Kumar, D. Burns, D. Dutta, and C. Hoffmann. A framework for object modeling. *Computer-Aided Design*, 31:541–556, 1999.

[19] C. Lim, G. M. Turkiyyah, M. A. Ganter, and D. W. Storti. Implicit reconstruction of solids from cloud point sets. In *Proceedings of the Third Symposium on Solid Modeling and Applications*, pages 393–402. ACM Press, 1995.

[20] Hongye Liu, Wonjoon Cho, Todd R. Jackson, Nicholas M. Patrikalakis, and Emanuel M. Sachs. Algorithms for design and interrogation of functionally gradient material objects. In *Proceedings of ASME 2000 IDETC/CIE 2000 ASME Design Automation Conference*, Baltimore, MD, 2000.

[21] K. Matsui and K. Terada. Continuous approximation of material distribution for topology optimization. *International Journal of Numerical Methods in Engineering*, 59:1925–1944, 2004.

[22] S. Muraki. Volumetric shape description of range data using "Blobby Model. *Proceedings of the ACM SIGGRAPH Conference on Computer Graphics*, 25(4):227–235, July 1991.

[23] J. Nocedal and S. J. Wright. *Numerical Optimization*. Springer-Verlag, 1999.

[24] Y. Ohtake, A. Belyaev, M. Alexa, G. Turk, and H.-P. Seidel. Multi-level partition of unity implicits. *ACM Transactions on Graphics (TOG)*, 22(3):463–470, 2003.

[25] J. Pegna and A. Safi. CAD modeling of multi-model structures for freeform fabrication. In *In Proceedings of the 1998 Solid Freeform Fabrication Symposium*, Austin, TX, August 1998.

[26] W. H. Press, S. A. Teukolsky, W. T. Vetterling, and B. P. Flannery. *Numerical Recipes in C*. Cambridge University Press, second edition, 1992.

[27] X. Qian and D. Dutta. Design of heterogeneous turbine blade. *Computer-Aided Design*, 35:319–329, 2003.

[28] Alon Raviv and Gershon Elber. Three-dimensional freeform sculpting via zero sets of scalar trivariate functions. *Computer-Aided Design*, 32:513–526, 2000.

[29] A. Ricci. A constructive geometry for computer graphics. *Computer Journal*, 16(3):157–160, May 1973.

[30] V. L. Rvachev. *Geometric Applications of Logic Algebra*. Naukova Dumka, 1967. In Russian.

[31] V. L. Rvachev. *Theory of R-functions and Some Applications*. Naukova Dumka, 1982. In Russian.

[32] V. L. Rvachev and T. I. Sheiko. *R*-functions in boundary value problems in mechanics. *Applied Mechanics Reviews*, 48(4):151–188, 1996.

[33] V. L. Rvachev, T. I. Sheiko, V. Shapiro, and I. Tsukanov. On completeness of RFM solution structures. *Computational Mechanics*, 25:305–316, 2000.

[34] Vladimir V. Savchenko, Alexander A. Pasko, Oleg G. Okunev, and Tosiyasu L. Kunii. Function Representation of Solids Reconstructed from Scattered Surface Points and Contours. *Computer Graphics Forum*, 14(4):181–188, 1995.

[35] Benjamin Schmitt, Alexander Pasko, and Christophe Schlick. Constructive sculpting of heterogeneous volumetric objects using trivariate b-splines. *The Visual Computer*, 20(2):130–148, may 2004.

[36] J. A. Sethian. *Level Set Methods and Fast Marching Methods: Evolving Interfaces in Computational Geometry, Fluid Mechanics, Computer Vision, and Materials Science*. Cambridge University Press, 1999.

[37] J. A. Sethian and A. Wiegmann. Structural boundary design via level set and immersed interface methods. *Journal of Computational Physics*, 163(2):489–528, 2000.

[38] V. Shapiro. Real functions for representation of rigid solids. *Computer-Aided Geometric Design*, 11(2):153–175, 1994.

[39] V. Shapiro. Well-formed set representations of solids. *International Journal on Computational Geometry and Applications*, 9(2):125–150, 1999.

[40] V. Shapiro. A convex deficiency tree algorithm for curved polygons. *International Journal of Computational Geometry and Applications*, 11(2):215–238, 2001.

[41] V. Shapiro. Semi-analytic geometry with R-functions. *Acta Numerica*, 16:239–303, 2007.

[42] V. Shapiro and I. Tsukanov. Implicit functions with guaranteed differential properties. In *Fifth ACM Symposium on Solid Modeling and Applications*, pages 258–269, Ann Arbor, MI, 1999.

[43] V. Shapiro and I. Tsukanov. Meshfree simulation of deforming domains. *Computer Aided Design*, 31:459–471, 1999.

[44] O. Sigmund and J. Petersson. Numerical instabilities in topology optimization: A survey on precedures dealing with checkerboards, mesh-dependencies and local minima. *Structural Optimization*, 16:68–75, 1998.

[45] I. Tsukanov and V. Shapiro. The architecture of SAGE – a meshfree system based on RFM. *Engineering with Computers*, 18(4):295–311, 2002.

[46] G. Turk and J. O'Brien. Modeling with implicit surfaces that interpolate. *ACM Transactions on Graphics*, 21(4):855–873, October 1999.

[47] Luiz Velho, Jonas Gomes, and Luiz H. de Figueiredo. *Implicit Objects in Computer Graphics*. Springer, 2002.

[48] M. Y. Wang, X. M. Wang, and D. M. Guo. A level set method for structural topology optimization. *Computer Methods in Applied Mechanics and Engineering*, 192(1-2):227–246, 2003.

[49] S. Y. Wang and M. Y. Wang. Radial basis functions and level set method for structural topology optimization. *International Journal for Numerical Methods in Engineering*, 65(12):2060–2090, 2005.

[50] K. Washizu. *Variational methods in elasticity and plasticity*. Oxford, Eng. ; New York : Pergamon Press, 3rd edition, 1982.